**Regular Paper**

# A Weather-aware Microclimate Prediction using Measurements of Meteorological Observatory

Genki Nishikawa†, Takuya Yoshihiro‡,

†Graduate School of Systems Engineering, Wakayama University, Japan
‡Faculty of Systems Engineering, Wakayama University, Japan
{s226183, tac}@wakayama-u.ac.jp

***Abstract*** - Microclimates, the climate measurements near the ground, are helpful for agriculture, town management, etc. To measure microclimates such as temperature and humidity, it is necessary to locate sensors at all the observation points on the ground. However, its high cost makes it unfeasible to keep sensors installed at many points. Hence, although some studies use machine learning techniques to learn the effects of topography to predict microclimate, it is difficult to obtain sufficient data to predict microclimate measurement because of various factors that affect microclimate. In this paper, we extended the conventional method that used the differences in measurements between the nearby meteorological observatory and the observation point, and proposed two ways to predict microclimate more accurately; One is using weather classification, and the other is using the meteorological measurements such as sunlight strength and wind direction.

***Keywords***: IoT, microclimate prediction, town management, meteorology

## 1 INTRODUCTION

Microclimate is the climate observed in a small area near the ground. Microclimate data is useful in several applications. For example, cultivation management using the observed microclimate in farm field contribute to automation and increases agricultural crops. Also, urban microclimate data is useful to avoid the bad effect on our health such as heatstroke. Consequently, to grasp microclimate is important. Microclimate depends on the surrounding environment and it depends on locations [1]. Hence, although it is necessary to locate sensors at all the observation points on the ground in order to measure microclimate such as temperature and humidity, keeping sensors installed at many points is unfeasible due to its large cost. Therefore, some studies proposed methods to predict microclimate.

Ueyama proposed a method that uses machine learning technique to learn the effects of topography, and predict microclimate based on topographical map [2]. However, it is difficult to obtain sufficient amount of data to predict microclimate measurement because of a wide variety of factors such as shape, materials and colors of buildings that effect on microclimate as well as anthropogenic heat and plants effect on microclimate.

To solve the problem, Kumagai et al. proposed a method that predicts microclimate measurement at an observed point based on the difference between the observation values at the observed point and those of the nearby meteorological observatory [3]. However, this method has a problem. This method simply adds the average of the differences between the observed values at the same time of prediction time in past days to the observed values of the meteorological observatory, and thus the prediction accuracy is low.

In this study, we focus on the observation that the difference depends on weather. For example, difference between temperature observed on a road paved with asphalt and the temperature observed at meteorological observatory surrounded by lawn will depend on the amount of sunlight. In this paper, we focus on weather as an important factor that increase the prediction accuracy. Therefore, we propose weather-aware microclimate prediction methods that use weather classification and meteorological observation.

The remainder of the paper is organized as follows. In section 2, we describe related work. Section 3 describes our method and materials. Section 4 presents the evaluation methods and results with our method. In section 5, we provide conclusions.

## 2 RELATED WORK

### 2.1 Prediction Based on Machine Learning

Suzui at el. proposed a method that predicts microclimate with RNN (Recurrent Neural Network) based on the observed values at the prediction places and nearby meteorological observatory [4]. The method reflects the effect of surronding environment on the predicted values because it is based on the relation between the measurements at the prediction places and the nearby meteorological observatory. However, we need a large volume of learning data to use machine learning techniques, and observing micloclimate measurements at the prediction places for a long time is practically unfeasible.

### 2.2 Prediction Based on Topography Effects

Ueyama at el. proposed a method that predicts microclimate by learning the effects of topography [2]. The method is mainly for farm fields including mountain areas, and predicts the highest and the lowest, and the average temperature of each day based on topography for each square area of the 10 meter grid of a map. In this study, they assume to install environmental sensors at several square cells, and utilize the dif-

ferences between the observation values of the cells and that from the nearby meteorological observatory. The study computes the difference in temperature according to several features in topography as the explanatory variables to estimate the effects of topography on temperature by means of stepwise regression. Then, they predict temperature for all cells based on the difference. In their evaluation, they installed sensors at 22 places, and predicted the highest and the lowest temperature, and the average of each day in each cell. As a result, the RMSE (Root Mean Square Error) values of the daily average temperature at the observed places was 0.8 °C, that of the highest temperature was 1.4 °C, that of the lowest temperature was 1.2 °C, respectively. Their RMSE might be considered a little large because the RMSE value of the pinpoint prediction provided by Japan Meteorological Agency is 1.5 °C.

### 2.3 Predicting Based on Meteorological Observatory

Kumagai at el. proposed a method that first observes microclimate at several prediction places, and predicts the microclimate measurements using the difference between the observed values at the prediction places and that of the nearby meteorological observatory at each predefined time segment [3]. In this study, their method predicts microclimate of each time segment by adding the differences of each time segment to the observed values of the meteorological observatory. Consequently, if we install a sensor at a prediction place for a certain period of time, we can predict the microclimate measurements at the place even after the sensor is removed. However, although the difference depends on weather and surrounding environment, this study do not take it into account. Hence, there is room for improvement.

## 3 PROPOSED METHOD

### 3.1 Overview

In this study, we propose a method that predicts microclimate with higher accuracy than the existing methods by extending the method of Kumagai et al. [3]. The conventional method predicts the differences between the observation values of the meteorological observatory and the microclimate measurements at each prediction time by calculating the average of the differences at the same time in the past days. Then, this method adds the differences to the observation values of the meteorological observatory for each prediction time to predict the microclimate measurements. We propose a method that predicts the differences with higher accuracy than the conventional method to improve the microclimate prediction accuracy. We observed the measured data and found that the difference between the observation values at the prediction places and that of the nearby meteorological observatory have different trends depending on weather. Accordingly, our method predicts the differences of the observation values between the prediction places and the nearest meteorological observatory at each prediction time by utilizing the trend of differences.

In Japan, meteorological measurements should generally be made in accordance with the Japan Meteorological Agency's guidebook [6] in order to avoid environmental influences. However, microclimate measurements are inevitably affected by the environment, equipment, installation methods, and other factors. In other words, the prediction of microclimate measurements must take all of these influences into account. Therefore, in this study, we predict the measurements when the same equipment is installed in the same location in the same manner as during the period of the learning data. This assumption, which is common to both our method and [3], is valid and appropriate because all those effects are included in the past observation data to be learned.

Figure 1 shows the common process of both our methods and the existing method [3] that predicts the microclimate measurement by using the predicted differences at each prediction time. Specifically, Fig. 1 shows an example of the microclimate prediction process for a day at a prediction place in a farm. We predict the microclimate measurements of the day at the prediction place from the observation data of the nearest meteorological observatory and the past measurements at the prediction place. The upper charts on the left of this figure show the time series microclimate observations at the prediction place in the past $k$ days, and the lower charts show the time series observations of the meteorological observatory in the past $k$ days. Our method predicts the differences using those observation values of the $k$-day learning period. The lower chart on the right of this figure shows the predicted differences of the prediction day, and the middle chart shows the observation values of the meteorological observatory of the prediction day. Our method and [3] add them together at each time of day to obtain the microclimate prediction, resulting in the graph on the upper right.

As written above, our method predicts microclimate measurements at a prediction place from the observation data of the nearby meteorological observatory and the past observation data at the prediction place. This is useful because we can predict microclimate measurements at the prediction place even after we remove the sensor at the prediction place. Note that it takes costs to maintain sensors long time. The proposed method enables us to obtain measurements for a long time by placing a sensor at the prediction place for a limited time period.

In this study, we propose two methods to predict the differences of the observation values to improve the prediction accuracy. The first method predicts the differences by using the weather classification obtained from the website. The second method predicts the differences by using the meteorological observation values such as sunlight strength, wind direction, and wind speed of the meteorological observatory. Note that the first method is applicable only if some weather report is available, whereas the second method requires specific measurement values. Users can make a good prediction using only weather reports, and can make a better prediction if specific measurement values related to sunlight and wind are available.

Note that the prediction steps shown in Fig. 1 is common among [3] and our proposed methods. The difference is the

algorithm to compute the "difference" between measurements of the meteorological observatory and of the sensor located at the prediction place, which is shown in Fig. 1 as "predicts the differences of the prediction day." The specific difference is shown in the following.

**Kumagai et al. [3]:** The differences are computed by averaging the past differences between the meteorological observatory and the sensor at the prediction place.

**Proposed method 1:** The differences are computed by taking into account weather reports to make better prediction accuracy.

**Proposed method 2:** The differences are computed by using specific data measured by the meteorological observatory, etc., to further improve the accuracy.

The procedures of our first method are as follows. In the first step of our first method, we install the environmental sensors and observe microclimate for a certain period of time as learning data for the prediction places. In addition, we calculate the differences of the observed values between prediction places and the nearby meteorological observatory. The second step of this method classifies weather of each observed time and extracts the differences if the weather is the same as the prediction time. Finally, the method calculates the average of the extracted differences to predict the differences at the prediction time.

The procedures of our second method are as follows. The first step of our second method is the same as the first method. This step observes microclimate for a certain period of time as learning data for the prediction places and calculates the differences of the observed values between prediction places and the nearby meteorological observatory. The second step of this method obtains 5 kinds of meteorological observation values, i.e., sunlight strength, wind direction, wind speed, relative humidity and air pressure measured at the prediction place or the nearest meteorological observatory. Here, we define the distance between observation time point and prediction time point as the euclid distance in the 5-dimensional space. Finally, the method predicts the difference for the prediction time by using the differences computed from the time points whose distance in the 5-dimentional space is relatively low.

## 3.2 Microclimate Prediction Method

We assume to install the environmental sensors and observe microclimate for a certain period of time at the place for prediction. Then, we remove the sensors to observe the microclimate and predicts the microclimate measurements from this time on. We represent an observation time by $t$ and a prediction place by $p$. Additionally, we represent the microclimate measurement at the prediction place $p$ at the time $t$ by $v^t$ and the observation value at the nearest meteorological observatory at time $t$ by $V^t$. Let the time to predict the measurement be $t'$. Our method predicts the difference $S_p^{t'}$ between $v^{t'}$ and $V^{t'}$ by using the differences $S_p^t$, where $t$ is included in the period of learning data, to predict the unknown microclimate measurement at time $t'$. In this study, we propose two methods to predict $S_p^{t'}$ by utilizing the trend of $S_p^t$ depending on the weather on the microclimate measuremenrs in the period of learning data.

The first method predicts the differences based on the weather classification obtained from such as weather forecast. The second method predicts the differences by using the meteorological observation values such as sunlight strength, wind direction, and wind speed. Note that the observation values are more detailed than the weather classification. According to the conventional study [3], it is effective to predict the microclimate from the differences of almost the same time in the past days. Hence, our methods uses the differences of almost the same time in the past days. In this study, we use the differences computed for the time in between before 30 minutes and after 30 minutes of prediction time $t'$ in the each past observation day. We specifically describe the methods to predict the difference $S_p^{t'}$ at time $t'$ in subsection 3.2 and 3.3.

We predict the microclimate measurements by using the differences $S_p^t$ depending on the two methods. If we obtain the observation values of the meteorological observatory $V^{t'}$, we obtain the prediction value $e_p^{t'}$ for the prediction time $t'$ and the prediction place $p$ from the following equation (1).

$$e_p^{t'} = V^{t'} + S_p^{t'}. \tag{1}$$

## 3.3 Calculating Differences Based on Weather

In this subsection, we describe a method to predict $S_{t'}$ based on the weather classification, which we can obtain from such as weather forecast. This method predicts the differences based on the weather classification that we can commonly available. Since the difference has different trends depending on weather, our method extracts the differences at the time points when the weather is similar to the prediction time $t'$ and also the time in a day is close to $t'$, in the past observation days. Our method calculates the average values of the extracted differences and uses the average values as the predicted difference of prediction time $t'$.

Specifically, this method predicts the difference $S_{t'}$ in equation (1) shown in Section 3.2 by using the weather classification. This method predicts the difference at time $t'$ based on the differences computed for each time in between before 30 minutes and after 30 minutes of prediction time $t'$ in each past observation day. More specifically, we denote the time $t$ of day $d$ by $t_{(d)}$, the number of past observation days by $k$, and the time we extracted from by $t \in [t_{(d)} - 30, t_{(d)} + 30], d = 1, 2, \ldots, k$, where the unit of time is a minute. Our method classifies the weather of each of the time $t$ and prediction time $t'$ into the 3 classes, i.e., sunny, cloudy, and rainy based on the weather forecast. We denote the weather of time $t$ by $w(t)$ and the set of time $t$ included in the same weather class as the prediction time $t'$ by $X$. Let the difference of the measurements between the prediction place $p$ and the nearest meteorological observatory at time $t$ by $D(p, t)$. We obtain the $S_p^{t'}$ from the following equation (2).

$$S_p^{t'} = \frac{1}{|X|} \sum_{t \in X} D(p, t) \tag{2}$$

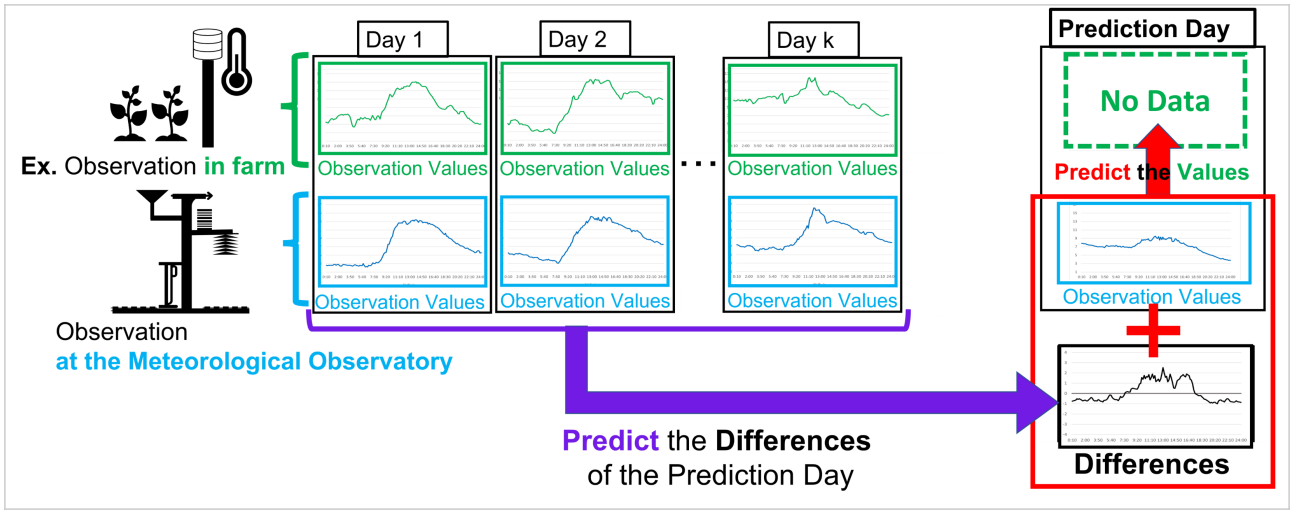


Figure 1: Overview of Predicting Microclimate

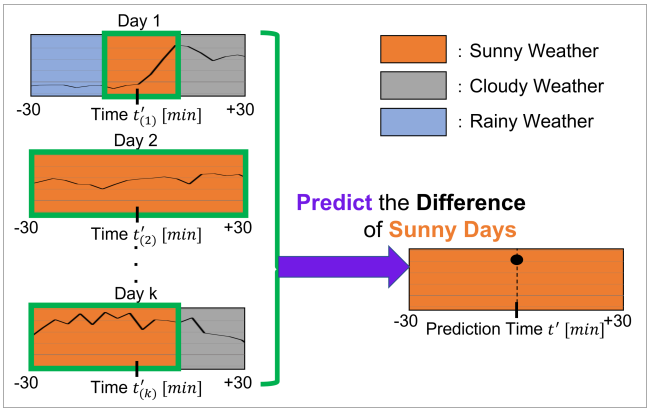


Figure 2: Predicting the Difference of Sunny Days

We show an example of predicting the difference in Fig. 2. Figure 2 shows the process to predict the difference at time $t'$ in a sunny day based on the measured differences between the predicting place $p$ and the nearest meteorological observatory in the past $k$ days. The back ground colors of the charts in this figure show the weather classes of each time, i.e., sunny, cloudy, and rainy weather obtained by the weather forecast. Each of the orange, gray, and blue parts shows the sunny, cloudy, or rainy weather. Three charts in the left-hand side show the time series of the measured differences in the time in between before 30 minutes and after 30 minutes of time $t'$ in each of the past $k$ observation days. This method extracts the differences of the time where weather is the same as that of prediction time $t'$. The time of which we extract the differences are shown by the green square in this figure. This method predicts the difference at the prediction time $t'$ shown in the right-hand side based on the extracted differences.

## 3.4 Calculating Differences Based on Meteorological Measurements

In this subsection, we describe the method to predict the difference $S_p^{t'}$ by using the meteorological observation values such as sunlight strength, wind direction, and wind speed. In this study, we focus on the meteorological observation values in addition to the weather as important factors that effect on the differences. We observed the differences and the meteorological observation values, and found that the difference has different trends depending on the observation values. Therefore, we propose a method that predicts the differences by using the meteorological observation values. That is, if the observation values are available, more accurate prediction will be possible.

Specifically, the prediction method in this section predicts $S_p^{t'}$ for prediction time $t'$ based on the differences computed for the time in between before 30 minutes and after 30 minutes in prediction time $t'$ in each of the $k$ past observation days. More specifically, we denote the time $t$ of day $d$ by $t_{(d)}$, the number of past observation days by $k$, and the time we extracted from by $t \in [t_{(d)} - 30, t_{(d)} + 30], d = 1, 2, \ldots, k$, where the time unit is a minute. In addition to the differences, this method uses the meteorological observation values, i.e., sunlight strength, wind direction, wind speed, relative humidity, and air pressure, observed in the area that contains both the prediction place and the meteorological observatory at the same time $t$. Since the differences between two time points tend to be small if those five meteorological observation values take similar values, this method extracts the differences of the $n$-nearest neighbor time points in the 5-dimensional space in which all time points in the $k$ days are plotted. From those $n$-nearest time points, we predict the difference of time $t'$.

In this paper, the meteorological observation values that we used are sunlight strength [lx], wind direction $[16 - \mathrm{Directions}]$, wind speed [m/s], relative humidity [%], and air pressure [hPa], observed by the meteorological observatory. We plot the observation values at time $t$ and prediction time $t'$ in the 5-dimensional space. Here, we define the distance between

time $t$ and prediction time $t'$ as the Euclid distance in the 5-dimensional space.

Assuming that those five meteorological observation values follows the normal distributions, we normalize the observation values to so that they are comparable among different dimensions. Specifically, we transform the observation values into the values whose standard deviation $\alpha$ is 0.5 and mean value is 0. This transformation standardizes the observation values, and multiplies the standardized values by 0.5 in order to adjust the interval $[-2\alpha, 2\alpha]$, namely, 95% confidence interval, to the interval $[-1, 1]$.

However, the wind direction values do not follow the normal distribution because the values are angles. Hence, we transform the wind direction values into the values between $-1$ and 1 by min-max normalization. Since d wind direction is a plane angle, the direction is represented in range $[r-\pi \leq \theta < r+\pi]$ where r is the given reference angle. In order to extract the neighborhood points of the prediction time point in the 5-dimensional space, we set r is the wind angle of the prediction point. Thus, we transform the wind direction value at prediction time into 0, and normalize the values of the other time points between $-1$ and 1 by the min-max normalization. Using those normalized meteorological observation values, this method calculates the distance between each time point $t$ and prediction time point $t'$ as the Euclid distance of their normalized values in the 5-dimensional space.

Figure 3 shows an example to extract $n$-neighborhoods where we consider 3-dimensional space for conciseness. We obtain the learning data for time $t'$ by extracting the $n$ time points $t$ in the ascending order of the distance from the prediction time $t'$. Plotted points in this figure shows meteorological measurement, and the colors of those points shows the variety of the measurements. The red point shows the measurement at prediction time $t'$, the purple points show the neighbor measurements of the red one, and the black points show the measurements in the learning data. The light yellow circle shows the neighborhood area of the prediction time $t'$.

Specifically, the obtained $n$ neighborhoods in the aforementioned 5-dimensional space are $n$ time points of the meteorological observatory measurements. Note that we assume those five dimensions, i.e., sunlight strength, wind direction, wind speed, relative humidity, and air pressure, are all observed at the meteorological observatory. (Note that, in our evaluation in Sec. 5, sunlight strength occasionally is not available at the nearest meteorological observatory, and we used the values observed at the prediction area.) We denote this set of time points by $Y = \{t_1, t_2, \ldots, t_n\}$. This method calculates the difference for the prediction time $t'$ based on $Y$ from the following equation,

$$S_p^{t'} = \frac{1}{|Y|} \sum_{t \in Y} D(p, t), \tag{3}$$

where, we denote the differences between the meteorological observatory and the prediction place $p$ at time $t$ by $D(p, t)$.

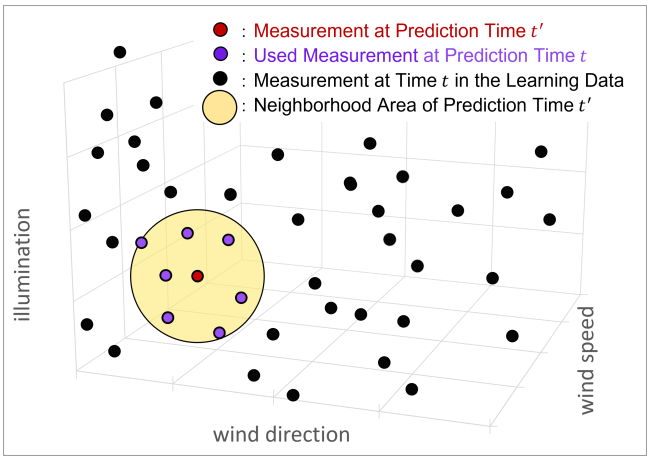


Figure 3: Data Extraction in 3D Space

# 4 EVALUATION

## 4.1 Evaluation Method

We installed sensors 2JCIE-BL [5] made by OMRON and observed microclimate at the seven prediction places around a building in Wakayama University for 234 days from February 4 to August 25, 2021. Afterwards, we predicted the temperature as a microclimate measurement to compare RMSE and MAE(Mean Absolute Error) of errors among our two methods and the conventional method [3]. Hereafter, we refer to our methods described in the section 3.3 and 3.4 as "Proposed1" and "Proposed2." Proposed1 estimates the differences of the observation values between prediction places and the nearest meteorological observatory by using the weather classification. Proposed2 estimates the differences by using five kinds of meteorological observation values, i.e., sunlight strength, wind direction, wind speed, relative humidity, and air pressure. Figure 4 shows the seven prediction places in the map around the building of Wakayama University. The nearby meteorological observatory is Wakayama Local Meteorological Observatory. Accordingly, we use the five kinds of meteorological observation values of the local meteorological observatory. We put the sensors in the solar radiation shields to shelter the sensors from the direct effect of sunlight, wind, and rain as shown in Fig. 5. According to the Japan Meteorological Agency's guidebook [6], in meteorological observation, we installed the sensors 1.5 m above the ground to avoid the direct effect from the ground to the sensors. The guidebook is not for microclimate; however, we installed the sensors 1.5 m above the ground with a tripod because the effect of the ground is too strong in temperature measurement. We attached weights to the tripod to prevent it from tipping over or moving. The condition of the tripod was checked frequently, particularly during strong winds. If it tips over or moves, we exclude the anomalous measurement data and return it to its original location. In this way, we maintained the correctness of the data.

The measurement time interval of the sensors was 1 minute. The measured values fluctuate with time as random measurement errors. Hence, we took the moving average with the 10-minutes window, as the 10-minute duration is the mea-

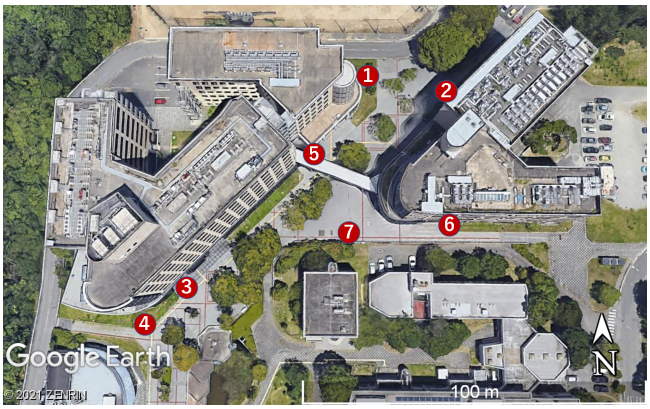


Figure 4: Observed Points ( Source: Google Earth )

surement time interval of the meteorological observatory to remove the fluctuations.

In this paper, we used the sunlight measured by the sensors at the prediction places around Wakayama University because, unfortunately, Wakayama Local Meteorological Observatory does not measure the sunlight. Since the relative sunlight strength is similar if the locations are close to each other, the sunlight strength measured at Wakayama University will be applicable. Although the sensors were in the solar radiation shields, the solar radiation shields cannot completely shelter the sensors from sunlight, and our sensors measure indirectly the strength of sunlight. Hence, we can obtain the relative sunlight strength by measuring the sunlight strength at Place 6, which always is not in the shade even when the sun is at its lowest elevation in a day. Note that cloud has a large effect on the sunlight strength, and the effect is fluctuated if the cloud is devided into small pieces. Additionally, sunlight belatedly affects the microclimate because the effect is indirect through the ground warmed by the sunlight energy. Therefore, we use the average of the last 1-hour sunlight strength as the sunlight strength at that time, instead of using the instant value at the time.

We used leave-one-out cross-validation in which we predict microclimate measurements in each of the prediction days based on the dataset excluding the measurements in the prediction day. We used the data of 1 month before and after each prediction day because our methods and the conventional method do not take seasonal variations into account. Specifically, we predicted the temperature measured at each prediction place and each time in each day of our observation period from the observation data of 1 month before and after each prediction day.

## 4.2 Preliminary Analysis

Prior to the evaluation of our method, we observed the relationship between the differences and the five kinds of meteorological measurement to evaluate the predictability. Specifically, we observed scatter plots whose vertical axis shows the differences, and horizontal axis shows each meteorological measurement, for each prediction places. As a result, we found that the differences have different trends depending on the meteorological measurements. Figures 7 (a)-(c) show the

Figure 5: Observation Device

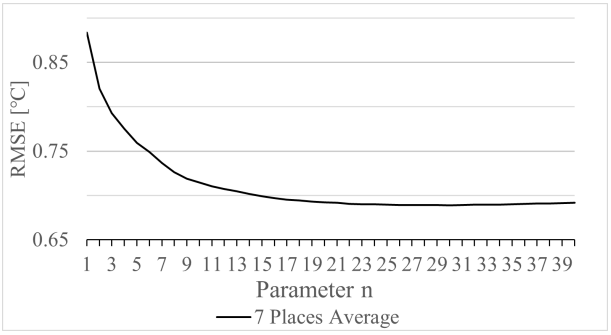


Figure 6: 7 Places Average of RMSE

scatter plots for Place 4 which notably show the result. Their vertical axes show the differences. The horizontal axes of the chart (a), (b), and (c) in the Fig. 7 show the sunlight strength, the wind direction, and the wind speed. Figure 8 shows a boxplot of the observation values for reference.

Figure 7 (a) shows the differences with the sunlight strength. We see that the differences correlate with the levels of the sunlight strength. Figure 7 (b) shows that the differences are in a large range between -2 and 4 °C when the wind direction is east-northeast or west-southwest and in a small range between -2 and 0 °C when the wind direction is approximately south. Figure 7 (c) shows the differences are approximately -1 °C only when the wind speed is 7.5 m/s or over. The differences of all places also have different trend depending on the meteorological measurements, which are similar to the case as the Place 4.

As the result, we concluded that the trends of the differences are similar when the meteorological measurements such as the sunlight strength, the wind direction, and the wind speed takes similar values. Therefore, we expect to improve the prediction accuracy by using the differences of the time points that have similar meteorological measurements to the prediction time points.

The parameter $n$ in Proposed2 is the number of differences used to predict each microclimate measurement. Although the parameter $n$ is an important factor to determine the ac-

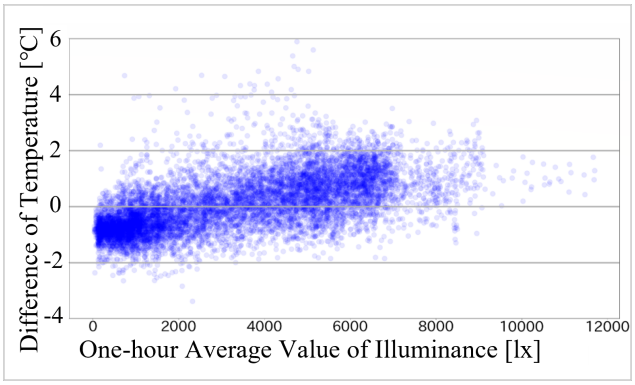


(a) Difference with Illuminance

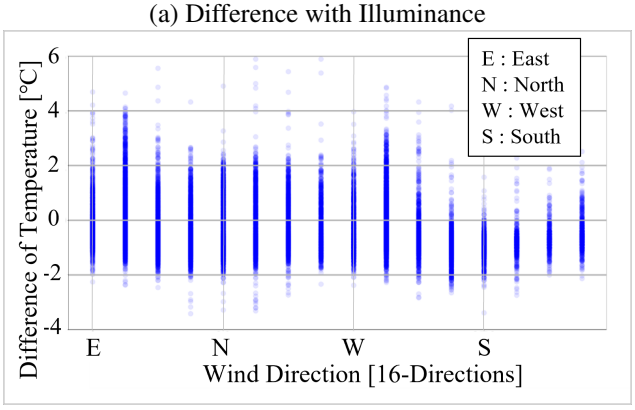


(b) Difference with Wind Direction

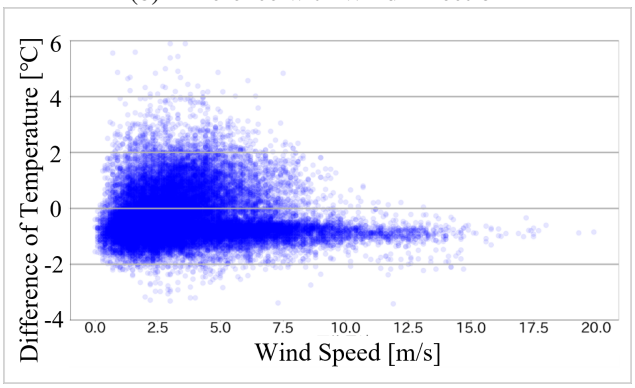


(c) Difference with Wind Speed

Figure 7: Scatter Charts of Difference and Observations

curacy, to determine $n$ logically is difficult. Therefore, in this study, we predicted the microclimate measurements using each natural number of $n$ and used the value that minimizes the average of RMSE. Figure 6 shows the average of RMSE values when $n$ is in between 1 to 40, which shows that the average of RMSE values decreases when $30 \leq n$ and increases when $n > 30$. Hence, we use the value $n = 30$ in our evaluation.

## 4.3 Evaluation Results

Figure 9 shows the prediction errors of the conventional method and our two methods. Figure 9 (a) shows the errors in RMSE at each prediction places and their average. Figure 9 (b) shows those errors in MAE. Although the errors have fluctuations depending on places, the errors of the Proposed1 are totally smaller than that of the existing method at

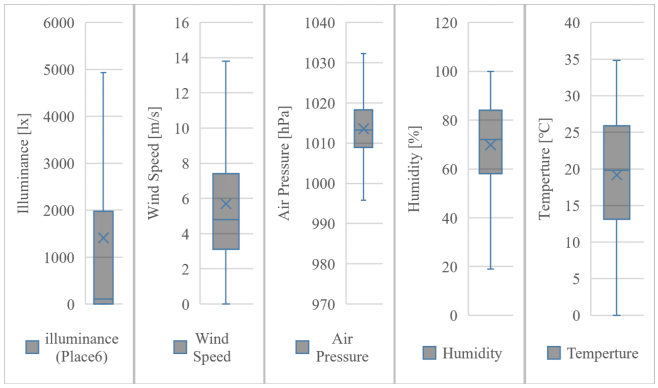


Figure 8: Boxplot of Observation Values

all places, and the errors of the Proposed2 are smaller than the Proposed1. Remember that the conventional method predicts the microclimate only based on the differences, but Proposed1 predicts it by using the weather classification, and Proposed2 predicts by using the meteorological observation values. As the results, if the weather classification is available, Proposed1 is the better prediction than the conventional method, and, if the meteorological observation values are available, Proposed2 is the better prediction than Proposed1.

Figure 10 shows those RMSE values at each prediction time segment from 0:10 to 24:00. Figure 10 (a), (b) and (c) show the RMSE values at each prediction place with the conventional method, Proposed1 and Proposed2 respectively. Figure 11 shows the relative RMSE of our methods based on the RMSE of the conventional method, namely, if the RMSE of the proposed method is the same as the conventional one, the value is 1.0. We found that the prediction errors at night time varies little among methods and places, but the errors during the daytime vary greatly regardless of methods and places. Additionally, at Places 1 and 5, the prediction error of Proposed1 is similar to that of the conventional method, meaning that weather classification is not effective for those places. Both of those places are under tree branches or buildings and are concluded to be less affected by sunlight. Therefore, Proposed1 predicts microclimate with higher accuracy than the conventional method mainly for the places where the sunlight has large effect.

Contrary to those places, at Places 3 and 6, Proposed1has much smaller errors than the conventional method. Although most of the prediction places are located between two buildings and thus tend to be windy, Place 3 and 6 is less windy because those locations are at the front porch or not in between buildings. Therefore, we conclude that the errors are relatively small because the places are less affected by the wind and have small temperature fluctuations.

Comparing Figures 11 (a) and (b), we found that the Proposed1 improves the accuracy only during the daytime, while the Proposed2 improves it even during the nighttime. Especially, we improve the prediction accuracy by about 40% in the daytime at the prediction place. At any time point, including nighttime, Proposed2 improves the prediction accuracy by about 10-30%. From these results, we concluded that Proposed2 can improve the prediction accuracy including nighttime by using the meteorological observations, i.e., sunlight

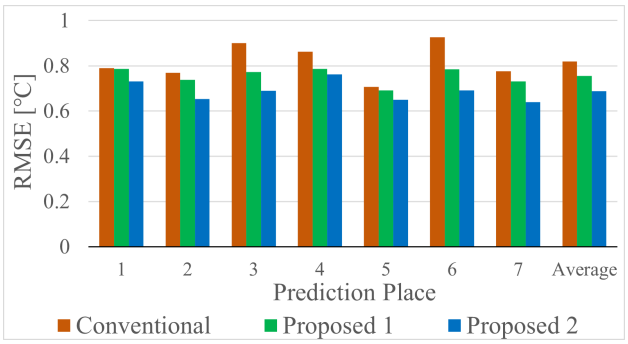


(a) RMSE

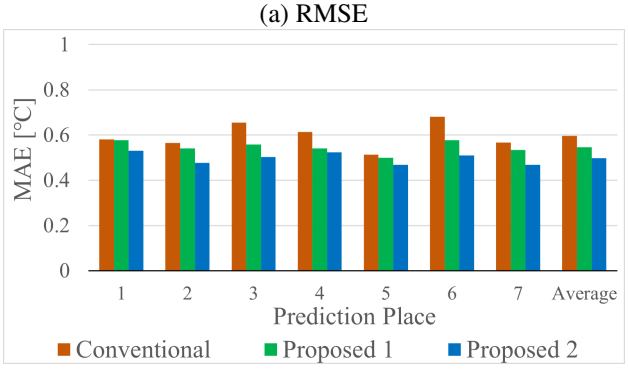


(b) MAE

Figure 9: Prediction Accuracy of each Place

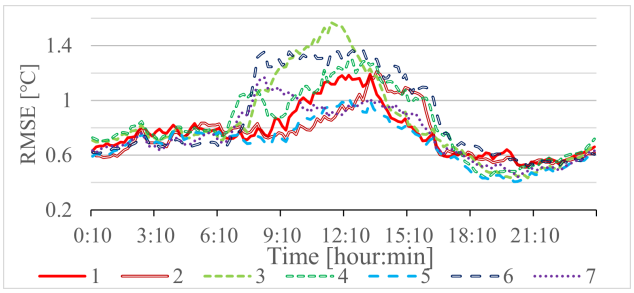


(a) Conventional Method

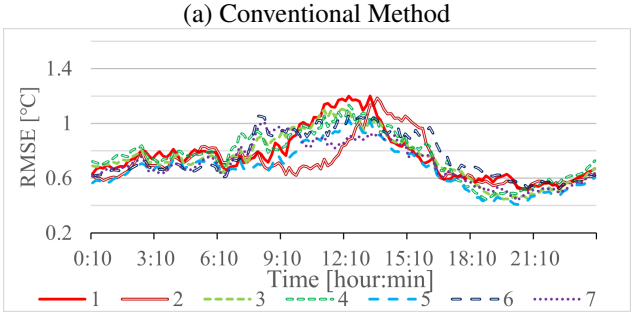


(b) Proposed Method 1

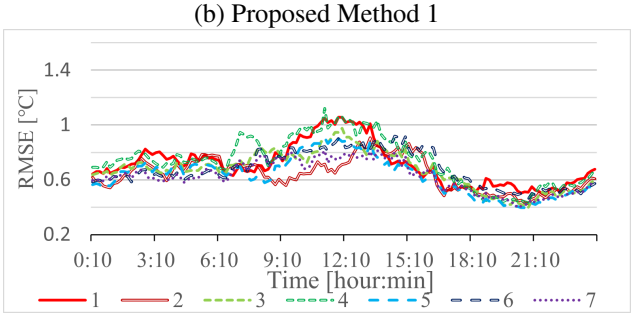


(c) Proposed Method 2

Figure 10: RMSE in time Series

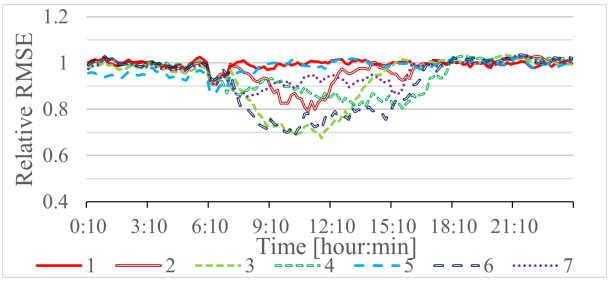


(a) Proposed Method 1

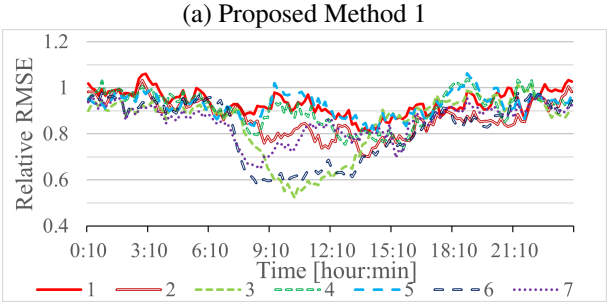


(b) Proposed Method 2

Figure 11: Relative RMSE in time Series

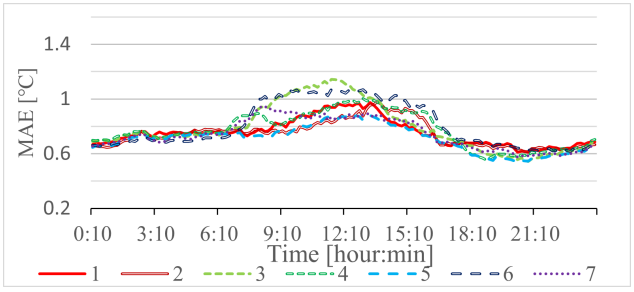


(a) Conventional Method

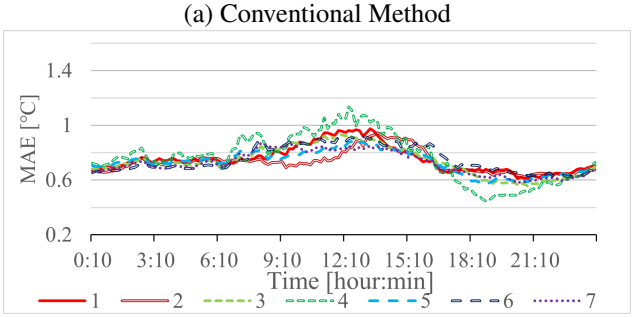


(b) Proposed Method 1

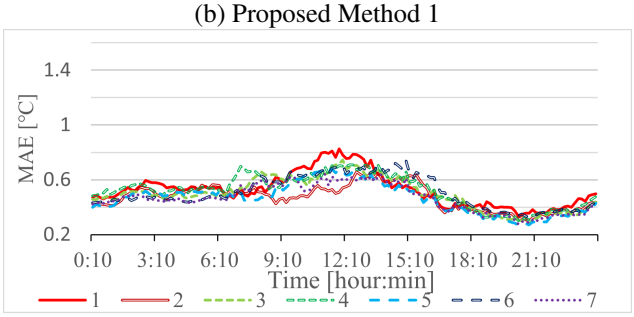


(c) Proposed Method 2

Figure 12: MAE in Time Series

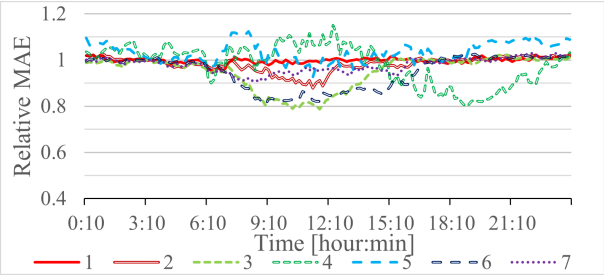


(a) Proposed Method 1

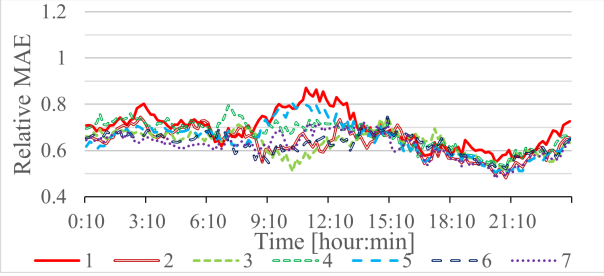


(b) Proposed Method 2

Figure 13: Relative MAE in Time Series

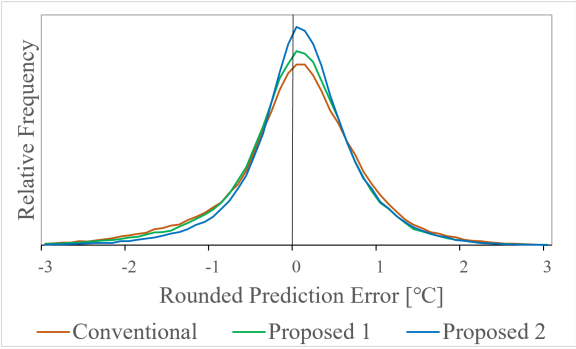


Figure 14: Relative Frequency Distribution

strength, wind direction, wind speed, relative humidity, and air pressure.

Figure 12 and 13 show the errors of Fig. 10 and Fig. 11 using MAE instead of RMSE. Comparing the errors of MAE in Fig. 13 (a), we find that the Proposed1 sometimes has a larger error than the conventional method. Note that the smaller RMSE with larger MAE means that the improvement in average is small, but extremely large error values are decreased. Therefore, we see that Proposed1 reduced the extremely large error values compared to the conventional method. In contrast, we find that the Proposed2 greatly improves the MAE including nighttime in Fig. 13 (b). In other words, Proposed1 improves prediction accuracy by reducing large errors, and Proposed2 improves the accuracy by improving the average errors.

Figure 14 shows the relative frequency distribution of the prediction errors. The horizontal axis shows the prediction errors rounded to the second decimal place, and the vertical axis shows the relative frequency of each rounded value. We found that Proposed1 has the prediction errors slightly smaller than that of the conventional method, and Proposed2 has the prediction errors that is slightly smaller than that of Proposed1.

Table 1: Characteristics of 7 places

| Place | Description |
|---|---|
| 1 | Located under a small tree, with poor sunlight throughout the day because of two high buildings. The ground is grass and not paved.<br>Temperatures are similar to those of the weather station at dawn, and lower than those of the weather station at other times of the day. The temperature difference from the weather station increases from morning to evening, and decreases toward dawn. |
| 2 | Direct sunlight only when the sun's altitude is high or the sun's direction is southwest. The ground is grass and not paved.<br>The lowest temperature among the 7 places is observed during the daytime. Temperatures tend to be similar to those of Place 1, with a few hours of higher temperatures in the late afternoon. |
| 3 | No sunlight in the west. Wind is weak among the seven sites because placed at the enterance of the building. The ground is paved with stones.<br>The second highest temperature among the seven stations is observed during the daytime. Temperatures are lower than those of the weather station from evening to midnight because of surrounded stones. |
| 4 | No sunlight from the southwest when the sun's altitude is low. The ground is grass and not paved.<br>Higher temperatures than the weather station are observed during the daytime. |
| 5 | Under a footbridge as a roof, without daylight all day. The ground is paved with stones.<br>Highest temperatures among the seven stations are observed from late at night to early in the morning. At other times of the day, temperatures are lower than those of the weather station. |
| 6 | No shade all day because of low buildings on the south side. Wind is weak among the seven sites.<br>The highest temperatures are observed during the daytime among the seven sites due to the influence of sunlight. The temperature rises the fastest and drops the latest among the seven sites. |
| 7 | The site is further away from high buildings than other sites. The site receives only southeast exposure when the sun's altitude is low. The ground is paved with stones.<br>The temperatures are always around the average of all the 7 sites. Temperatures are higher than those of the weather station in the morning and lower at other times of the day. |

Table 1 shows the characteristics of these seven sites. Places 4 and 6 have high buildings to the north (about 30 m and 23 m, respectively), which provide shade in many places. On the other hand, the buildings on the south side of places 4, 7, and 6 are all low (under 5 m), allowing sunlight to reach the site from the south. As a result, as shown in Fig. 9, 10, etc., places 3, 4, and 6 have relatively long sunlight hours, resulting in large prediction errors. The proposed method is particularly suited to reduce the error due to such sunlight effects.

## 5 CONCLUSIONS

We proposed two weather-aware microclimate prediction methods that predict microclimate measurements based on the differences between the past measurements at the prediction place and that of the nearby meteorological observatory. One of our methods utilizes weather classification to predict microclimate measurements, and the other utilizes multiple meteorological measurement values.

We evaluated our methods using a data set measured nearby Wakayama University. Specifically, we measured microclimates at seven prediction places around a building of Wakayama

University for 234 days. As a result, we showed that both of our methods outperform the conventional method, and among the two proposals, the method based on meteorological measurements has higher performance than that based on simple weather classification. It means that, if detailed data is available, better prediction of microclimate is possible.

In future work, it would be important to analyze the seasonal effect in order to reduce the amount of data for microclimate prediction. Knowing the relationship among different microclimate measurements also will contribute to data reduction and performance improvements.

## REFERENCES

[1] Ministry of the Environment, Heat Illness Prevention Information, 〈https://www.wbgt.env.go.jp/wbgt.php〉 Referred in October 2022 (in Japanese).
[2] H. Ueyama, ”Developing Applications to Create 50m-mesh Data of Temperature, Sunlight Strength, Relative Humidity, Reference Evaporation”, Bulletin of the NARO Agricultural Research for Western Region, Vol. 19, pp. 13-43 (2019) (in Japanese).
[3] K. Kumagai, T. Uchibayashi, T. Abe, T. Suganuma, ”Predicting Microclimate from Sensor Data for Town Management”, IPSJ SIG Technical Report, , Vol. 2016-IS-138 No.10, pp. 1-7 (2016) (in Japanese).
[4] S. Suzuki, N. Fujiki, ”Prediction and Supplement of Meteorological Data Using Recurrent Neural Networks”, The 82nd National Convention of IPSJ, pp. 285-286 (2020), (in Japanese).
[5] Omron, 2JCIE-BL01 Environment Sensor, 〈https://www.omron.co.jp/ecb/product-info/sensor/iot-sensor/environmental-sensor〉 Referred in October 2022 (in Japanese).
[6] Japan Meteorological Aency, ”A Guidbook for Meteorological Observation”, 〈https://www.jma.go.jp/jma/kishou/know/kansoku_guide/guidebook.pdf〉 Referred in October, 2022 (in Japanese).

(Received October 11, 2022)
(Accepted May 22, 2023)

**Genki Nishikawa** is a graduate student of Graduate School of Systems Engineering, Wakayama University, Japan. He received the B.E. degree from Wakayama University, in 2021. His research interests include IoT and meteorology. He is currently with Core Corporation.

**Takuya Yoshihiro** is an associate profesor of Faculty of Systems Engineering, Wakayama University, Japan. He received the B.E., M.I., and Ph.D. degrees from Kyoto University, in 1998, 2000, and 2003, respectively. He was an Assistant Professor at Wakayama University, from 2003 to 2009, where he has been an Associate Professor, since 2009. He is currently interested in graph theory, distributed algorithms, computer networks, wireless networks, medical applications, bioinformatics, IoT, and data ecosystems. He is a member of ACM, IEICE, and IPSJ.

**Regular Paper**

# Pedestrian Cooperative Autonomous Mobility
# -Path Planning Adapted to Pedestrian Face Direction-

Yuto Yada*, Shunsuke Michita*, Seiji Komiya* and Toshihiro Wakita*

*Graduate School of Engineering, Kanagawa Institute of Technology, Japan
s2284001@cco.kanagawa-it.ac.jp

***Abstract*** - Autonomous mobility in mixed traffic environments with pedestrians need functions to avoid contact with pedestrians. In this study, path planning method adapted to pedestrian face direction was developed. For pedestrians who are aware of mobility (forward facing walking), small avoidance path is generated. For pedestrians who are unaware of mobility (downward facing walking), such as those who are walking on their smartphones, large avoidance path is generated. Subjective evaluation experiments were conducted on four items: distance, speed, smoothness of avoidance, and reliability. The subjective evaluation results showed that the evaluations improved for all items except speed, both for forward and downward walking. In particular, for downward facing pedestrians the evaluation of the distance was considerably improved. In addition, objective evaluation indicators corresponding to the subjective evaluations were examined.

***Keywords***: Autonomous Mobility, Pedestrian behavior prediction, Yolo

## 1 INTRODUCTION

In recent years, the practical application of autonomous mobility has been progressing worldwide in areas such as office building security and package delivery. Autonomous mobility moves in mixed traffic environments with pedestrians need a path planning function that avoids contact with pedestrians. When humans pass each other, they unconsciously make eye contact with each other and anticipate the other's movements to ensure smooth movement. Therefore, we are working on the realization of autonomous mobility that enables this type of behavior.

DWA (Dynamic Window Approach) [1] and RRT (Rapidly exploring random tree) [2] have been widely used as static obstacle avoidance methods for mobile mobility. The problem with these previous studies was that dynamic obstacles such as pedestrians could not be avoided because they were not considered.

For dynamic obstacle avoidance, pedestrian prediction using the Kalman filter [3], pedestrian prediction and avoidance using the potential method [4], and the application of ORCA (Optimal Reciprocal Collision Avoidance) to the prediction and avoidance of multiple pedestrians [5] have been studied.

One of the problems for previous studies is avoidance for pedestrians walking on their smartphones. It is difficult for mobility to avoid pedestrians walking while gazing at their smartphones. This is because their walking path is unstable and behavior prediction is difficult. Also, pedestrians walking on their smartphones may be surprised when mobility suddenly appears in their field of vision when they pass by at close range while they are gazing at their smartphones. To solve the problem, a method of warning by sound can be considered. Although pedestrians may notice mobility with sound warnings, this method causes mobility to impede pedestrians' walking, and frequent warning sounds can make pedestrians uncomfortable. Especially when autonomous mobility increases in the future, it is unlikely that autonomous mobility will always be prioritized over pedestrians. As another means, a method of large avoidance can be considered. Although the method could avoid the pedestrian safely, such large avoidance would be excessive for pedestrians walking forward. If excessive avoidance is always performed, there is a high possibility that it will take a long time to arrive at the destination or the route cannot be generated and the mobility cannot move. Pedestrians appear to avoid other pedestrians according to their characteristics.

Therefore, in this study, a method to adjust the amount of avoidance according to the face direction was attempted. After predicting the pedestrian's behavior, the risk of collision is reduced by avoiding a small amount when the pedestrian's face is in front of the vehicle and a large amount when the face is facing downwards. Despite avoiding pedestrians using this method, if a collision is unavoidable, the mobility stops. This avoidance strategy is similar to that used by humans every day.

## 2 PEDESTRIAN BEHAVIOUR EXPERIMENTS

Pedestrian trajectory measurement experiments were conducted to see how pedestrians avoid each other.

The experiment was conducted on 12 subjects. Each subjects were asked to walk at a natural speed and pass opposite pedestrians. The starting position was completely face each other and the walking distance was 10 m.

An example of pedestrian trajectory against a forward-facing pedestrian is shown in Fig. 1. And an example of pedestrian trajectory against a downward-facing pedestrian is shown in Fig. 2.

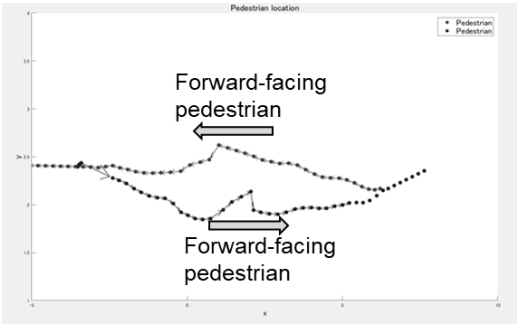


Figure 1: An example of pedestrian trajectory against a forward-facing pedestrian.

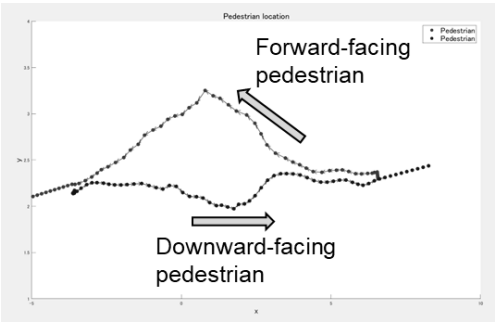


Figure 2: An example of pedestrian trajectory against a downward-facing pedestrian.

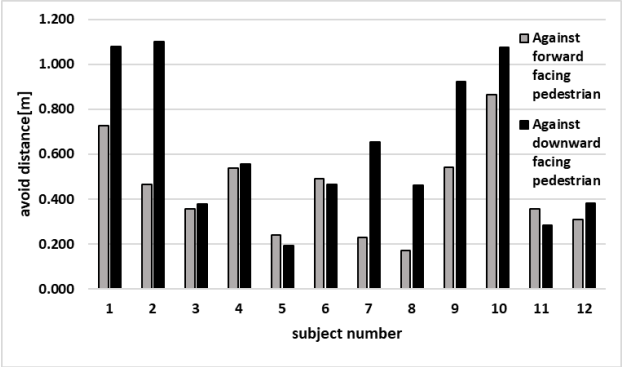


Figure 3: The avoidance distance result.

The amount of avoidance against forward-facing pedestrians and the amount of avoidance against downward-facing pedestrians were compared. The amount of avoidance is shown in Fig. 3.

Significant difference tests were conducted paired t-test with a significance level of 0.01 and a null hypothesis of 'no difference in mean values between the two groups. The two groups are the amount of avoidance against forward-facing pedestrians and the amount of avoidance against downward-facing pedestrians. The results of the significance difference test showed a p-value of 0.0077, with a significance level of 1%. This shows that pedestrians, on average, largely avoid other pedestrians who are downward-facing pedestrian. Therefore, in this research, an attempt was made to realize such human behavior in autonomous mobility.

# 3 METHOD

To safely avoid a downward-facing pedestrian, the face direction of the pedestrian is recognized by face direction recognition. Next, if the result of the face direction is a downward-facing pedestrian, a large avoidance path is generated. We considered these two requirements for pedestrian avoidance.

The method is based on the following procedure.

Step1 Measurement of pedestrian position using 3D LiDAR, pedestrian detection, tracking, and pedestrian behavior prediction.

Step2 Pedestrian face direction detection by image recognition .

Step3 Collision risk area calculation based on the pedestrian behavior prediction and pedestrian face direction detection results.

Step4 Pedestrian avoidance route generation.

A schematic diagram of the proposed algorithm is shown below (Fig. 4).

As in previous studies [3], 3D LiDAR information and a Kalman filter were used for pedestrian recognition and pedestrian behavior prediction.

## 3.1 System Configuration

The autonomous mobility used in this experiment is shown in Fig. 5. It was equipped with a camera for face direction detection of pedestrians and an omnidirectional laser sensor for self-localization and obstacle detection. Data obtained from these onboard devices is processed and controlled by a compact computer DH310 (Shuttle) and a Jetson Xavier NX (NVIDIA) (Table. 1).

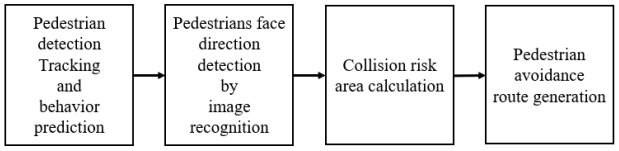


Figure 4: Method of pedestrian cooperative path planning.

Figure 5: Mobility.

Table 1: System Configuration.

| | |
|---|---|
| Camera | C920n web camera (Logicool) |
| LiDAR | VLP-16 (Velodyne) |
| Computers | DH310 (Shutlle) |
| | Jetson Xavier NX (NVIDIA) |

## 3.2 Face Recognition

To estimate whether pedestrians are aware of autonomous mobility or not, this study assumes that pedestrians whose faces are forward-facing are aware of autonomous mobility and those whose faces are downward-facing are not aware. Pedestrian face direction recognition was performed using deep learning with Yolo [6]. An example of recognition is shown in Fig. 6. First, 300 images were taken of each pedestrian with a forward face and a downward face. Next, 4000 epochs of deep learning by Yolo were performed using the collected images. The recognition rate of forwarding-facing was about 99% and that of downward-facing was about 77% (Table. 2).

## 3.3 Path Planning

Route generation was performed by RRT* [7] based on the occupancy grid map.

Based on the results of pedestrian face direction recognition and pedestrian behavior prediction, collision risk areas were defined on the occupancy grid map used in route generation (Fig. 7). For pedestrian behavior prediction, the walking speed of the tracked pedestrian was calculated using a Kalman filter, and the predicted position was calculated based on the calculated walking speed.

The width of the collision risk area is the same as the width of the body when avoiding a forward-facing pedestrian (hereinafter referred to as 'small avoidance'), and is wider when avoiding a downward-facing pedestrian (hereinafter referred to as 'large avoidance') so that a safe distance is maintained between the pedestrian and the collision risk area. The collision risk area was treated like an obstacle in the route generation.


Figure 6: Recognized example of face direction.

Table 2: Recognition result of face direction.

| | | Recognition result | |
|---|---|---|---|
| | | Forward | Downward |
| Human behavior | Forward | 99% | 1% |
| | Downward | 23% | 77% |

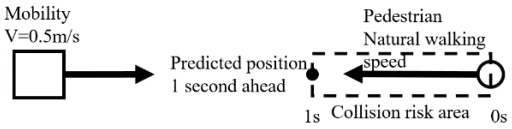


Figure 7: Collision risk area.

# 4 EXPERIMENS AND RESULTS

Using the proposed path planning algorithm, a subjective evaluation experiment on pedestrian avoidance was conducted in a laboratory. A course was created as shown in Fig. 8, and the autonomous mobility was moved at a translational velocity of 0.5 m/s. Pedestrians were instructed to walk at their natural walking speed and evaluate whether the autonomous mobility could avoid pedestrians.

## 4.1 Path Planning Results

The path planning results are shown below. For comparison, similar experiments were conducted under path planning without behavior prediction. Three types of path planning were used: without behavior prediction (Fig. 9), small avoidance (Fig. 10), and large avoidance (Fig. 11). The bold lines are the selected paths and the branches are the candidate paths. It was confirmed that the system generated a largely avoidable path for downward-facing pedestrians compared to forward-facing pedestrians.

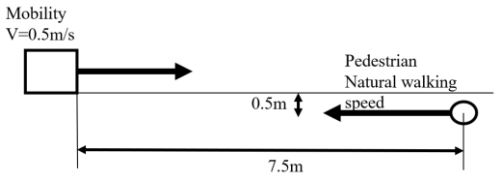


Figure 8: Layout of pedestrian avoidance experiment.

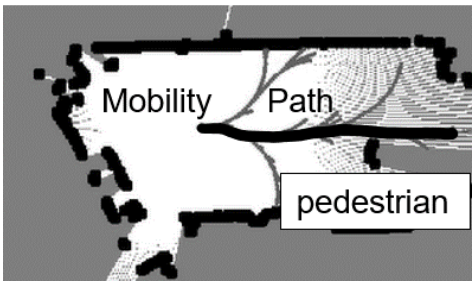


Figure 9: Path planning example of without behavior prediction path planning. The bold line represents the selected path and the branch line represent candidate path.

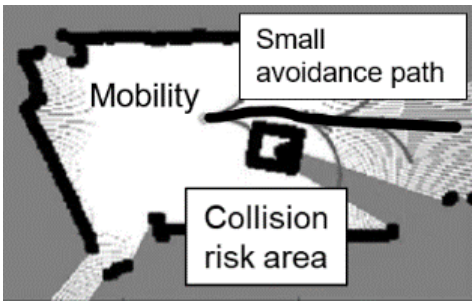


Figure 10: Path planning example of small avoidance cooperative path planning. The bold line represents the selected path and the branch lines represent candidate path. The square represents the collision risk area.

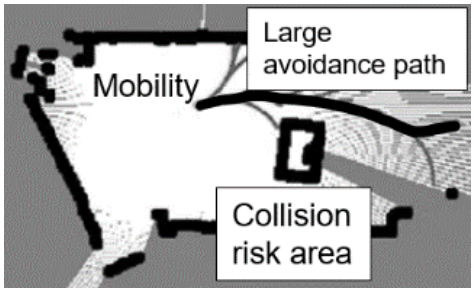


Figure 11: Path planning example of large avoidance cooperative path planning. The bold line represents the selected path and the branch lines represent candidate path. The square represents the collision risk area.

Figs 12, 13, and 14 show the trajectory examples for without behavior prediction, small avoidance, and large avoidance, respectively.

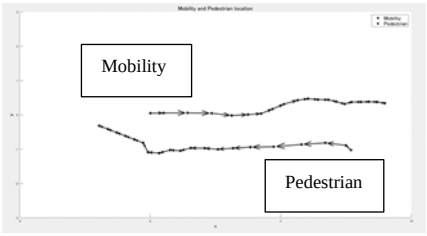


Figure 12: Trajectory example of without behavior prediction path planning.

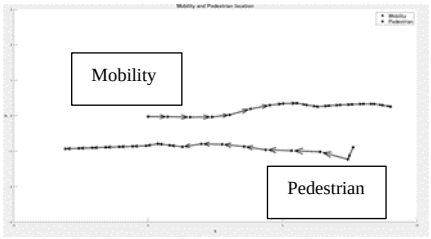


Figure 13: Trajectory example of small avoidance cooperative path planning.

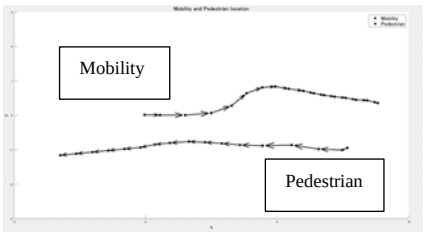


Figure 14: Trajectory example of large avoidance cooperative path planning.

The paths also showed that large avoidance was avoided to a greater extent than small avoidance and that the timing of avoidance was delayed without the collision risk area.

## 4.2 Subjective Evaluation Results

Subjective evaluation of pedestrian avoidance performance was carried out on nine subjects. In the experiment with 12 subjects in Chapter 2, it was shown that there was a significant difference between the trajectories of avoidance against forward-facing pedestrians and those against downward-facing pedestrians. Therefore, a more detailed experiment on avoidance with mobility was conducted with nine subjects. Two trials of each condition were made to each subject. Experiments were carried out based on the approval of the Human Ethics Review Committee of Kanagawa institute of technology.

Subjective evaluation was performed with 4 evaluation items. They are "distance from the autonomous mobility when passing by", "speed of the mobility when passing by", "smoothness of passing by (avoidance performance)", and "reliability when passing by". These items were evaluated in five levels, with the following ratings: 'good', 'a little good', 'undecided', 'a little bad', and 'bad'.

Subjective evaluation results are as follows (Figs. 15 and 16). In the case of forward-facing pedestrians, the evaluation of all items improved in comparison without behavior prediction and small avoidance. In the case of downward-facing pedestrians, the evaluation values of all items improved in comparison without behavior prediction and large avoidance. Especially, in the case of downward-facing pedestrians, the evaluation of distance was considerably improved. No change was observed in the evaluation of speed, partly because the vehicles were driven at the same speed in all three conditions.

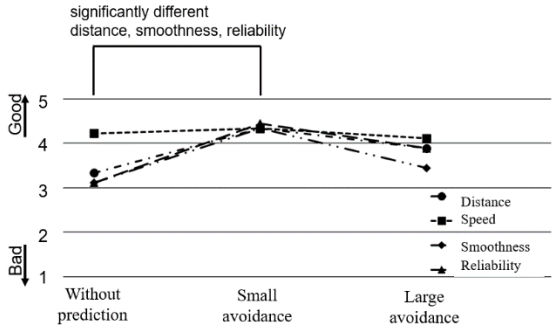


Figure 15: Subjective evaluation results for conscious pedestrians.

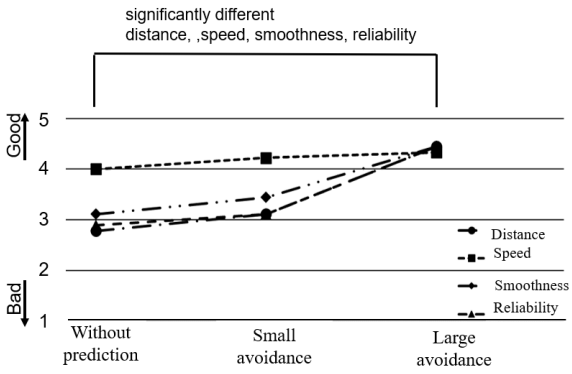


Figure 16: Subjective evaluation result.

Significant difference tests were conducted paired t-test with a significance level of 0.05 and a null hypothesis of 'no difference in mean values between the two groups. In this study, method of successive categories was used to convert subjective evaluation results from ordinal scale to interval scales. Without behavior prediction and small avoidance were compared for forward-facing pedestrians, and without behavior prediction and large avoidance were compared for downward-facing pedestrians. The p-values for each item are shown below (Tables 3 and 4).

# 5 PHYSICAL INDICATORS

## 5.1 Objective Evaluation Results

The physical quantities corresponding to the four evaluation items “distance”, “speed”, “smoothness”, and “reliability”, which were considered to be related to passing each other, were examined.

First, we considered the item of "distance" when passing each other. In this study, the nearest neighbor distance at the time of passing was used as the distance perceived by the subjects. As an example, the distance was 0.83 m in the case of without behavior prediction, 1.05 m in the case of small avoidance and 1.45 m in the case of large avoidance.

Table 3: Result of significance test for forward facing pedestrian (* p<0.05).

| item | P-value |
|---|---|
| Distance | 0.043* significantly different |
| Speed | 0.173 |
| Smoothness | 0.057 significantly different |
| Reliability | 0.025* significantly different |

Table 4: Result of significance test for downward facing pedestrian (* p<0.05, ** p<0.01).

| item | P-value |
|---|---|
| Distance | 0.004** significantly different |
| Speed | 0.041* significantly different |
| Smoothness | 0.017* significantly different |
| Reliability | 0.005** significantly different |

Next, "speed" was examined. Relative speed and absolute speed can be considered as index candidates. In this study, the speed perceived by the pedestrian is considered as the relative speed of the mobility. The pedestrian was asked to walk at natural walking speed in all three conditions and the translational velocity of the mobility was constant for all three conditions. As an example, the relative velocity was 0.87 m/s in the case of without behavior prediction, 1.01 m/s in the case of small avoidance, and 0.93 m/s in the case of large avoidance.

“Smoothness” was further considered. The turning angular velocity ω during the avoidance is used as an indicator. The point where the angular velocity became 0.1 rad/s or bigger was defined as the avoidance start, and the angular velocity until it became less than 0.1 was averaged. In the case of without behavior prediction, no avoidance is performed, therefore the average value of the turning angular velocity reached to the nearest distance is used. As an example, the average value of the turning angular velocity during avoidance was 0.00 rad/s is for the without behavior prediction, 0.14 rad/s for small avoidance, and 0.29 rad/s for large avoidance.

## 5.2 Indicator for Reliability

A physical quantity that correspond to the "reliability" when passing each other was examined.

Time to collision (TTC) is a physical index used in the Autonomous Emergency Braking (AEB) installed in vehicles. This indicator represents the time until collision with the leading vehicle if the current relative speed of the leading vehicle to the ego vehicle is maintained. Let $x_e$, $v_e$, be the front end position and velocity of the ego vehicle and $x_l$, $v_l$ be the rear end position and velocity of the leading vehicle in the world coordinate system. In this case, the relative distance $d_x$ and the relative velocity $v_x$ of the leading vehicle relative to the ego vehicle are $x_l - x_e$, $v_l - v_e$ (Fig. 17). Therefore, if the value of TTC is $t_x$, the following equation is obtained (1).

$$t_x = -\frac{d_x}{v_x} = -\frac{x_l - x_e}{v_l - v_e} \quad (1)$$

In a previous study [8], it was shown that most people drive with a TTC of 4 seconds or longer. Therefore, TTC may be used as an indicator of reliability. In this study, a physical quantity by expanding the TTC to two dimensions (2D TTC) was investigated. In addition, pedestrians are assumed to be in constant velocity linear motion and mobility is assumed to have constant translational and rotational velocity.

The method for calculating 2D TTC is as follows. It was assumed that the pedestrian would move linearly at a constant velocity and the mobility would move at a constant translational velocity and a constant angular velocity. The coordinate transformation from the world coordinate system to the mobility coordinate system is performed. The positions and velocities of the autonomous mobility and pedestrian in the world coordinate system are shown in the Fig. 18. The position and speed of the mobility are $(x_e(t), y_e(t))$ and

$(v_{ex}(t), v_{ey}(t))$, and the predicted position and the predicted speed of the pedestrian are $(x_p(t), y_p(t))$ *and* $(v_{px}, v_{py})$. The distance from the center of gravity of the vehicle to the front center of the vehicle is $h$. The position and velocity of the pedestrian in the world coordinate system are transformed into the mobility coordinate system with reference to the mobility's center of gravity. In this case, the relative position $(x_r(t), y_r(t))$ and relative velocity $(v_{rx}(t), v_{ry}(t))$ of the pedestrian relative to the vehicle front of the mobility are $(x_p(t) - (x_e(t) + h), y_p(t) - y_e(t))$ *and* $(v_{px} - v_{ex}(t), v_{py} - v_{ey}(t))$ (Fig. 19).

The path distance $d_p$ is defined as the Equation (2). The path distance represents the distance from the current location to the collision point. $t_{collision}$ represents the predicted time when the collision would occur.

$$d_p(t) = \int_t^{t_{collision}} \sqrt{v_{rx}(t)^2 + v_{ry}(t)^2}\, dt \tag{2}$$

In addition, the absolute value of the relative velocity is given by equation(3).

$$v_r(t) = \sqrt{v_{rx}(t)^2 + v_{ry}(t)^2} \tag{3}$$

Therefore, if the value of the 2D TTC is $t_c$, it follows that equation(4).

$$t_c(t) = \frac{d_{p(t)}}{v_r(t)} \tag{4}$$

The value of the 2D TTC in the case of no collision is defined as infinite.

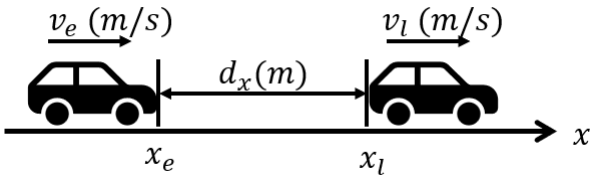


Figure 17:TTC outline figure.

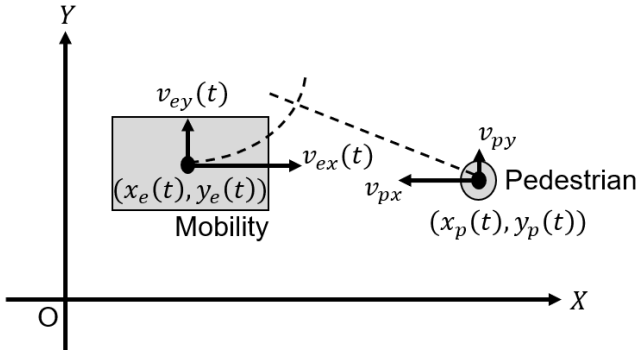


Figure 18:World coordinate system.

The 2D TTC was calculated for three conditions: without behavior prediction, small avoidance, and large avoidance. The mobility, pedestrian position and 2D TTC values during the calculation using MATLAB are shown (Figs 20, 21, and 22).

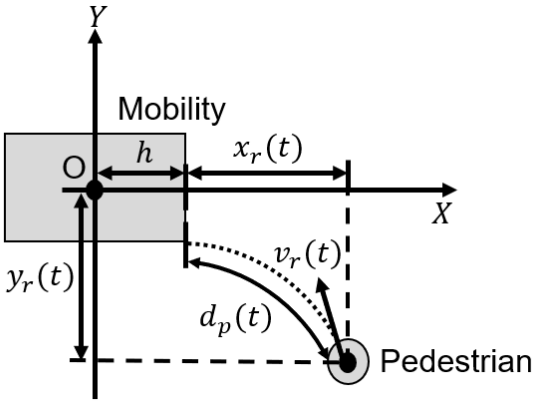


Figure 19: Mobility coordinate system.

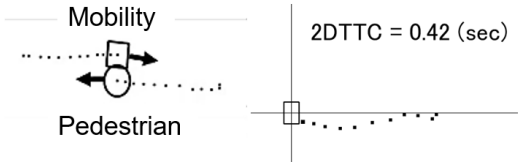


Figure 20: Without behavior prediction 2DTTC calculation diagram.

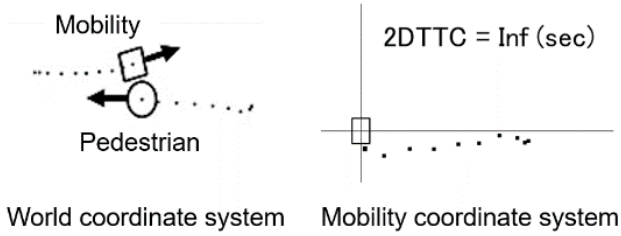


Figure 21: Small avoidance 2DTTC calculation diagram.

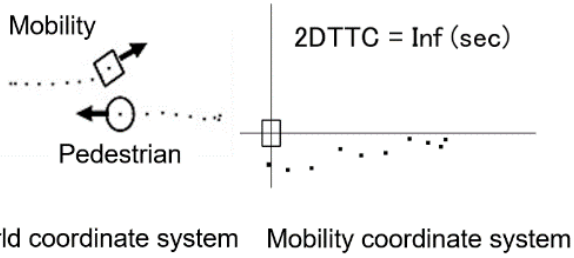


Figure 22: Large avoidance 2DTTC calculation diagram.

## 5.3 Example of Physical Indicators

An example of physical indicators value during forward-facing pedestrians is shown in the figure in chronological order (Fig. 23).

## 5.4 Relationship Between Subjective Evaluation and Physical Indicators.

The results for the subjective and objective evaluation values are shown in Figs 24, 25, 26, and 27.

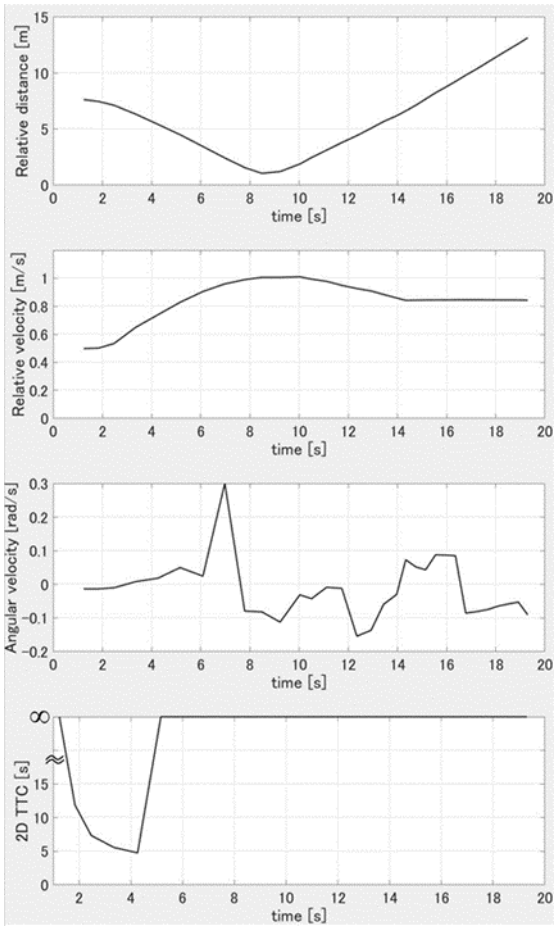


Figure 23: Example of physical indicators.

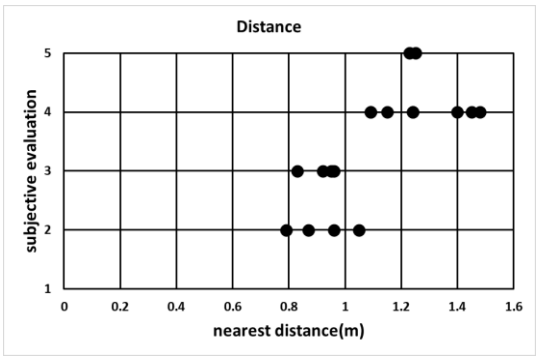


Figure 24: Relationships between distance and subjective evaluation.

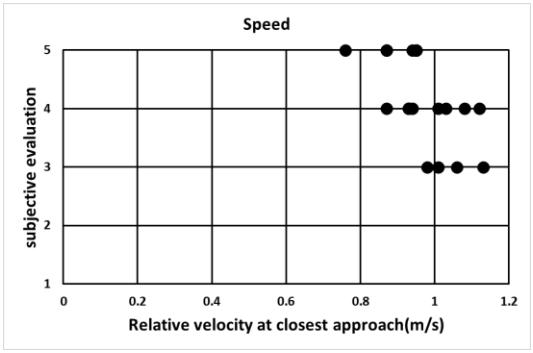


Figure 25: Relationships between speed and subjective evaluation.

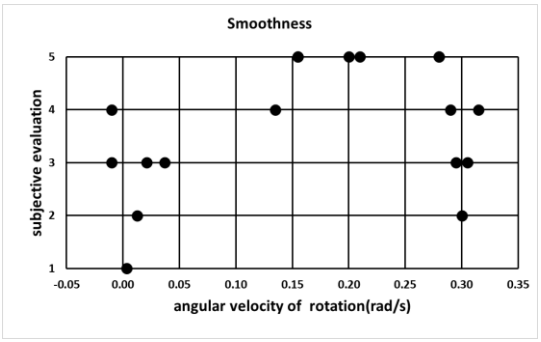


Figure 26: Relationships between smoothness and subjective evaluation.

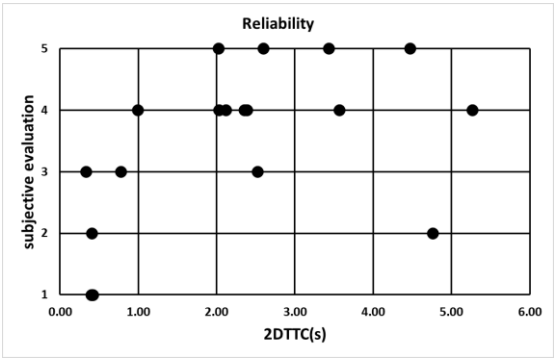


Figure 27: Relationships between reliability and subjective evaluation.

As for distance, the subjective evaluation value improves as the value of the closest neighbor distance increase.

For speed, the subjective evaluation value improves as the value of the relative speed at the closest approach decrease.

Regarding smoothness, the subjective evaluation value improves as the angular velocity of the turn increase.

The subjective evaluation value of the reliability worsens when the 2D TTC value is less than one second, while the subjective evaluation value improves when the 2D TTC value is two seconds or more.

# 6 DISCUSSION

## 6.1 The Results of the Subjective Evaluation.

Both forward and downward-facing pedestrians improved the subjective evaluation results for all items except speed. Speed was highly rated in all three conditions, with no significant differences observed. It is considered that this is because the mobility moved at a constant speed under all experimental conditions.

In the subjective evaluation of forward-facing pedestrians, the evaluation of large avoidance was slightly worse than that of small avoidance. Several subjects commented on the poor smoothness of large avoidance, such as "I felt poor smoothness" and "If I were a human, I would feel un-comfortable as if I were being large avoided". From this result, it seems that small avoidance is appropriate for for-ward-facing pedestrians.

Significant differences in distance and reliability were found for forward-facing walking. This result is thought to be due to the fact that the mobility without prediction (no collision risk area) pass pedestrians at a close distance, while those with a collision risk area maintain a certain distance while avoiding pedestrians.

In downward-facing walking, significant differences were observed in all items except speed. In forward-facing walking, the presence of mobility can be confirmed early on in the effective field of view, whereas in downward-facing walking, the effective field of view is narrower than in forward-facing walking because walking is done while gazing at the smartphone [9], and the pedestrian only confirms the presence of the mobility when it enters the peripheral field of view just before passing by. Therefore, the evaluation of distance, the reliability and smoothness decreased, whereas with the collision risk area, the reliability also improved because the robot maintains a maximum safe distance and makes a larger avoidance compared to forward-facing walking.

## 6.2 The Results of the Objective Evaluation.

With regard to the relationships graph for smoothness (Fig. 26), the subjective evaluation value largely changes at the small turning angle speed value. These conditions are path without behavior prediction and no avoidance is performed. Further studies are needed on these characteristics.

With regard to the relationships graph for the reliability (Fig. 27), there is an outlier where the subjective evaluation worsens despite the high 2DTTC value, but this is thought to be influenced by one subject's opinion that he felt nothing in particular about the reliability because he avoided the area a little himself. Overall, the subjective evaluation largely changes as the value of 2DTTC increased.

# 7 CONCLUSION

In this study, we proposed a path planning algorithm that adapts to the face direction of pedestrians and safely avoids pedestrians who are walking while on their smartphones.

Our subjective evaluation results suggest that there are relationships between the evaluation values and the physical indicators.

This method would enable the operation of advanced collaboration between pedestrians and autonomous mobility on campus.

# REFERENCES

[1] D. Fox, W. Burgard, and S. Thrun, "The dynamic window aproach to collision avoidance," IEEE Robot. Autom. Mag., Vol. 4, No. 1, pp. 23-33,(1997).

[2] S. M. LaValle, "Rapidly-Exploring Random Trees: A New Tool for Path Planning," Tech. Rep, (1998).

[3] T. Goto, "Pedestrian behavior prediction and forecast circle generation using Kalman filter"(2019).

[4] H. Hisahara et al, "Human Avoidance Function for Robotic Vacuum Cleaner Through Use of Environmental Sensors -Roomba® Making Way for Humans" , IEEE, Fifth International Conference on Intelligent Systems, Modelling and Simula-tion, pp.64-67.(2014).

[5] D. Zhang, Z. Xie et al,"Real-Time Navigation in Dynamic Human Environments Using Optimal Reciprocal Collision Avoidance", IEEE International Conference on Mechatronics and Automation.(2015).

[6] J. Redmon et al., "You Only Look Once: Unified, Real-Time Object Detection", 2016 IEEE Conference on Compute Vision and Pattern Recognition (2016).

[7] "Plan Mobile Robot Paths Using RRT", https://jp.mathworks.com/help/nav/ug/plan-mobile-robot-paths-using-rrt.html.

[8] C. Shibata et al, "Driver characteristic estimation using vehicle behavior fata while preceding vehicle decelerating", Information Processing Society of Japan (2016).

[9] D. Saito " Change in effective visual field using smartphone with walking" , Biomedical Fuzzy System Association (2019).

(Received: October 31, 2022)
(Accepted: June 4, 2023)

**Yuto Yada**
He was graduated from school of Vehicle System Engineering, Kanagawa Institute of Technology as a bachelor. Also, he is a master student at Graduate School of Mechanical system engineering, Kanagawa Institute of Technology, Japan. His expertise is development of intelligent mobility.

**Shunsuke Michita**
He was graduated from school of Vehicle System Engineering, Kanagawa Institute of Technology as a bachelor. Also, he earned his master's degree in the Department of Mechanical System Engineering from the Kanagawa Institute of Technology. He is currently employed at Honda Motor Co., Ltd.

**Seiji Komiya**
He was graduated from the Graduate School of Engineering, Yokohama National University in March 1990. Joined Kanagawa Institute of Technology, where he currently works. His expertise is the development of intelligent mobility.

**Toshihiro Wakita** received B.E. from Kyoto University, M.S. from The University of Tokyo and Ph.D. degree from Nagoya University in 1983, 1985 and 2006, respectively. He is currently a professor at Kanagawa Institute of Technology. His research interest includes intelligent mobility and human machine interface. He is a member of IEEE, JSAE, IEICE, and IPSJ.